Journal of Fish Diseases

WILEY

Journal of Fish Diseases

RESEARCH ARTICLE OPEN ACCESS

Hindcasting Farmed Salmon Mortality to Improve Future Health and Production Outcomes

Benjamin R. Knight[1,2] | Eric A. Treml[2,3] | Zac Waddington[4] | Ross Vennell[1] | Kate S. Hutson[1,5]

[1]Cawthron Institute, Nelson, New Zealand | [2]School of Life and Environmental Sciences, Deakin University, Geelong, Victoria, Australia | [3]AIMS the Australian Institute of Marine Science, Perth, Western Australia, Australia | [4]New Zealand King Salmon Company, Picton, New Zealand | [5]Centre for Sustainable Tropical Fisheries and Aquaculture, College of Science and Engineering, James Cook University, Townsville, Queensland, Australia

Correspondence: Benjamin R. Knight (ben.knight@cawthron.org.nz)

Received: 29 August 2024 | **Revised:** 7 November 2024 | **Accepted:** 21 November 2024

Funding: This work was supported by Cawthron Institute and Ministry for Business Innovation and Employment.

Keywords: aquaculture | aquatic disease | climate change | connectivity | modelling | salmon | vaccine

ABSTRACT

Intracellular, free-floating and biofilm-forming bacterial pathogens have been implicated in summer mortality of farmed Chinook salmon, *Oncorhynchus tshawytscha*, in New Zealand. A mortality event in 2022 in the Pelorus Sound, Marlborough, was linked to high water temperatures (> 18°C), and bacterial skin disease associated with *Piscirickettsia* spp. (=*Rickettsia*-like organisms) and *Tenacibaculum* species. To understand the progression of infection and potential drivers of the mortality, simulation of the event was conducted using a networked susceptible, infectious and recovered (SIR) model. Parameter exploration shows that reconstruction of observed mortality rates across three affected farm sites was possible. The best SIR simulations identified plausible values for key drivers of disease, which are consistent with previously estimated disease parameter ranges for *Piscirickettsia salmonis*. Our modelling shows the 2022 Pelorus Sound event likely experienced spread of bacterial pathogens within healthy fish populations at salmon farm sites over a 10-week long incubation period, before elevated mortality was observed. We show evidence that vaccine use at one site likely prevented 10% higher mortality and that an alternative site for the vaccination could have further reduced mortalities. This result highlights the importance of future vaccine developments in aquaculture and the potential to improve vaccine efficacy through considered site selection.

1 | Introduction

Disease incursions represent a threat to the growth and sustainability of global aquaculture (Bruno, Noguera, and Poppe 2013; Stentiford et al. 2017) and the ecosystems they inhabit (Bouwmeester et al. 2021; Harvell and Lamb 2020). There are predictions that disease-related mortality in aquaculture will increase globally due to intensification of the industry, emerging pathogens and increased thermal stress on cultured animals from a changing climate (Handisyde, Telfer, and Ross 2017; Combe et al. 2023; Reid et al. 2019). New Zealand aquaculture is experiencing similar climate challenges to the global industry, with warming water trends (Sutton and Bowen 2019) and emerging disease threats (Lane, Brosnahan, and Poulin 2020).

Chinook salmon, *Oncorhynchus tshawytscha,* aquaculture is the only farmed marine salmon in New Zealand, with its production comprising 75% of the global aquaculture market for the species (AQNZ 2024). Production of salmon in New Zealand predominantly occurs in the Marlborough Sounds and is divided between the estuarine Pelorus Sound in the west, and the cooler, more oceanic waters of Queen Charlotte Sound in the east (Figure 1).

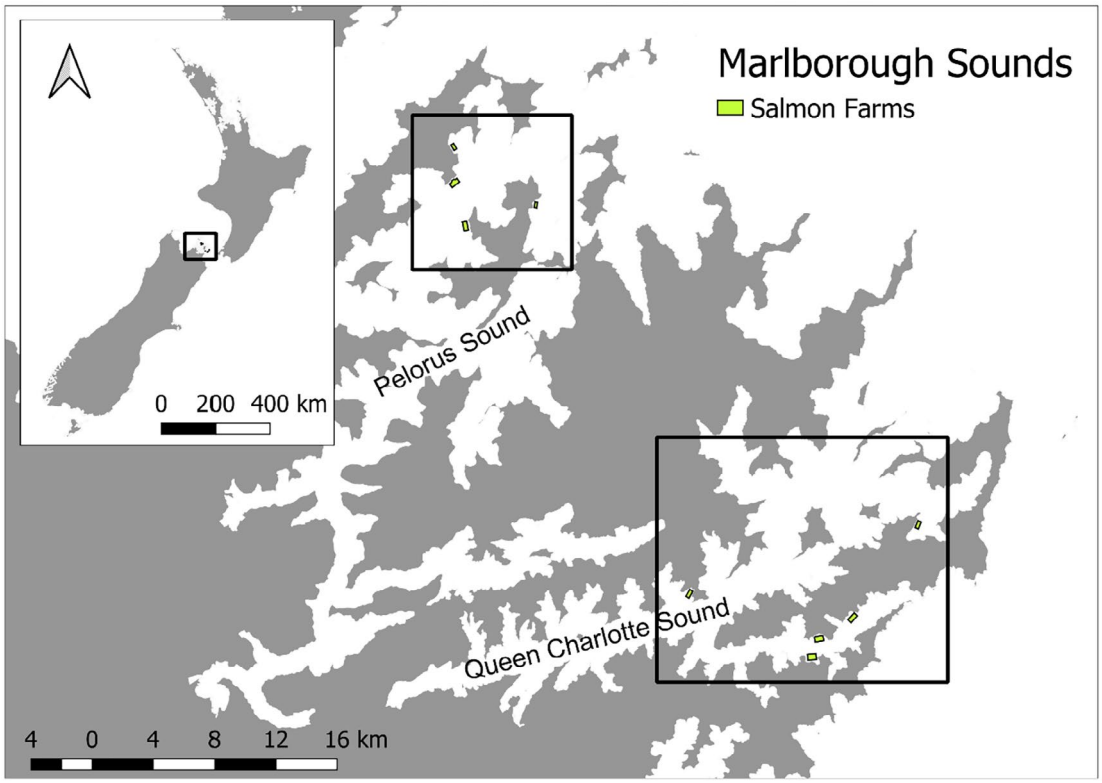

FIGURE 1 | The Marlborough Sounds, in New Zealand, showing the salmon farm sites (yellow boxes) in the main farming regions of the Pelorus and Queen Charlotte sounds (regions indicated by black boxes). Map projection: New Zealand Transverse Mercator 2000.

Cultured Chinook salmon farming has historically seen low disease–associated losses in New Zealand (Brosnahan et al. 2017; Monterey Bay Aquarium 2020). This is now changing, with an increasing number of new aquatic pathogens being reported (e.g., Lane, Brosnahan, and Poulin 2020; Kumanan et al. 2022). Investigations into recurrent summer mortalities in New Zealand salmon aquaculture commenced in 2015 and identified the presence of two potentially pathogenic bacterial species: *Piscirickettsia* spp. (= New Zealand *Rickettsia*-like organisms NZ-RLO1 and NZ-RLO2; Schober et al. 2023) and *Tenacibaculum maritimum* (previously *Flexibacter maritimus* / *Cytophaga marina*) (Brosnahan et al. 2017). More recent investigations also noted the presence of additional pathogenic *Tenacibaculum* species including *T. dicentrarchi*, *T. soleae* and *T. finnmarkense* (Kumanan et al. 2022).

Chinook salmon mortality events in the Marlborough Sounds prior to 2022 were found to be associated with high water temperatures, typically over 17.5°C (Brosnahan et al. 2017; Brosnahan, Munday, Ha, et al. 2019; Brosnahan 2020; Kumanan et al. 2022), which is a similar pattern to what has been observed globally in other bacterial mortality events (e.g., *P. salmonis* outbreak events in Atlantic salmon; Rozas and Enríquez 2014). At times, temperatures in Pelorus Sound during the 2022 mortality event exceeded 18.5°C, which can affect the survival of marine *O. tshawytscha* (Abdul-Aziz, Mantua, and Myers 2011; Marcoli et al. 2023). This indicates that marine climatic factors likely played a role in the pathogenicity of disease-causing organisms observed in the Marlborough Sounds (Brosnahan, Munday, Ha, et al. 2019).

We adopted a modelling approach to help understand complex interacting factors that could influence disease progression and mortality in Pelorus Sound and for use as a tool to reduce future losses. There has been no previous modelling of bacterial disease spread in salmon in New Zealand; however, modelling on *P. salmonis* was undertaken in Chile by Wada et al. (2021) and Bravo et al. (2020). Wada et al. (2021) used a commercially available disease simulation package to model susceptible and infected populations for three aquaculture species using a simple kernel density spread modelling approach. Similarly, Bravo et al. (2020) included simulation of a recovered population (i.e., an SIR model) incorporating a particle tracking approach to estimate farm connectivity. Consequently, the use of dynamic modelling to predict mortality from bacterial infection was adopted.

The aim of this study was to better understand the drivers of salmon summer mortality events and provide a tool to investigate management options to improve fish welfare and reduce future mortality. An assessment of vaccine efficacy was used to highlight the value of the tool for investigating future disease management. This was achieved through retrospective simulation of the Pelorus Sound salmon mortality event over the summer of 2021/2022 using a networked susceptible, infectious and recovered (SIR) modelling approach.

2 | Background

The 2021/2022 austral summer mortality event over the in Pelorus Sound resulted in the loss of 1300 t of salmon, or about 10% of New Zealand's annual production (Figure 2). The 2021/2022 Pelorus Sound mortality event was the largest

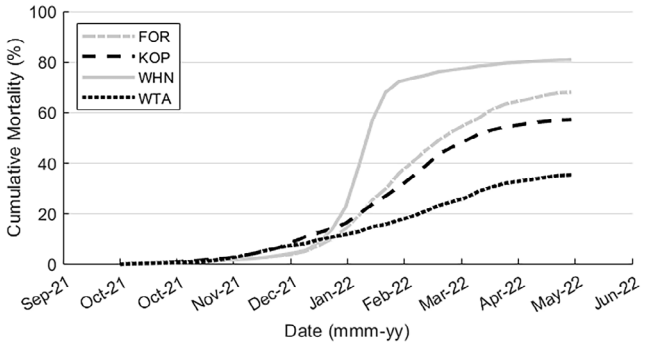

FIGURE 2 | Pelorus Sound cumulative mortality over the period 1 October 2021 to 30 May 2022 for the four Pelorus Sounds Salmon farms; KOP = Kopaua, FOR = Forsyth, WTA = Waitata and WHN = Waihinau. Data source: New Zealand King Salmon Limited.

observed in the region following two decades of salmon farming. The maximum weekly mortality at the worst-affected site, Waihinau, was about three times higher than the peak mortality at any other farm site despite having similar aged fish (one-year old) to most other sites. The exception was the Kopaua site, which had two-year-old fish.

The event was associated with NZ-RLO1 and *Tenacibaculum* sp. detection. NZ-RLO1 was suspected as a primary contributor to the mortality at the worst afflicted farm based on qualitative assessment of moribund fish by qualified individuals, and a wide range of testing including molecular and histological assessments during the peak of the mortality event (data not shown). Evidence for NZ-RLO1 as a major contributor to mortality at other farm sites in Pelorus Sound was not clear, based on investigations on moribund fish. Concurrent mortalities in Queen Charlotte Sound farm sites were associated with NZ-RLO2, but resulted in fewer mortalities. Due to the magnitude of the 2021/2022 Pelorus event and the large distance between the Pelorus and Queen Charlotte Sound farm sites, this study focusses only on modelling infection spread and the associated mortality at the Pelorus Sound farm sites.

The total relative mortality at the Waihinau site was also about 20% higher than any other farm site over the course of the event (Figure 2). The Waitata farm site was associated with comparatively low mortality rates, and differed from the other sites due the presence of inoculated fish with a bivalent vaccine for NZ-RLO1 and *T. maritimum* and higher current speeds. Higher mortalities may have also been prevented at the Kopaua site due to early detection of elevated mortalities and early harvesting of two-year-old fish. Other differences in husbandry and other environmental conditions existed between the sites. These differences included the use of bubblers, net cleaning frequency, current speeds, depths and the potential for different pathogens (including NZ-RLO1 and *Tenacibaculum* sp.) to be present across farm sites. Consequently, multiple factors likely contributed to differences in the observed mortality across the farm sites.

Two pathogenic NZ-RLO strains have been implicated in Chinook salmon mortality in New Zealand—NZ-RLO1 and NZ-RLO2—with a third strain, NZ-RLO3, isolated from fish that were not clinically diseased and from a region where summer mortalities were not recorded (Brosnahan 2020). Recent molecular investigations by Schober et al. (2023) found NZ-RLO2 grouped within established *P. salmonis* EM genogroup, but that NZ-RLO1 was only distantly related to established genogroups for *P. salmonis*. Piscirickettsiosis (also referred to as salmonid rickettsial syndrome or SRS) from Chilean strains of *P. salmonis* is one of the most important diseases affecting farmed salmon in that region (Rozas and Enríquez 2014; Bravo et al. 2020). Given the large amount of information available for this important pathogen and similarities with NZ-RLOs, it was chosen as a model pathogen for this study.

Tenacibaculum species have also been implicated in Chinook salmon mortalities in New Zealand (Brosnahan, Munday, Ha, et al. 2019; Kumanan et al. 2022). Tenacibaculosis occurs in many marine fishes with various gross clinical presentations including skin lesions, necrosis and tail rot (Devesa, Barja, and Toranzo 1989; Nowlan et al. 2021). In the Marlborough Sounds, Brosnahan, Munday, Ha, et al. (2019) showed that NZ-RLO1, NZ-RLO2 and *T. maritimum* were associated with fish exhibiting skin ulcers, and more recently, a disease investigation in 2020 reported 100% detection of *T. maritimum* in diseased fish (Kumanan et al. 2022), in the absence of NZ-RLOs. Known salmonid pathogens *T. soleae* and *T. dicentrarchi* were also detected. Subsequent fulfilment of Koch's postulates in a natural seawater challenge experiments for local strains of *T. maritimum* and *T. dicentrachi* under high concentrations ($>10^9$ CFU/mL) in Chinook salmon provides evidence that tenacibaculosis was likely a contributor to salmon mortality in the region (Unpublished data: Kumanan et al. 2024).

3 | Methods

The approach adopted for this study used a coupling between physical hydrodynamics, the movement of bacterial pathogens and the modelling of the SIR populations in each farm site. Chinook salmon farming in New Zealand occurs within defined sites consented to occupy and operate under Resource Management Act legislation (New Zealand Government 1991) and other associated regulations in a manner similar to the lease arrangements used in other countries. The term 'farm site' used in this study refers to a collection of pens within a single consented area; for the period considered here, fish were not physically moved between sites.

To derive the estimates of connectivity between farm sites, a physical hydrodynamic model was used to drive a Lagrangian particle tracking model that simulated the movement of pathogen material between farm sites (Bravo et al. 2020). The interfarm hydrodynamic connectivity and the time taken to transport pathogens between farm sites was estimated from the results of the particle tracking simulations. This underlying information was then used to construct a networked SIR model to simulate bacterial infections in Chinook salmon, its spread within salmon farms in Pelorus Sound and fish mortalities.

3.1 | Calculating Connectivity and Time-of-Travel

Transmission of pathogens has been shown to occur between distant salmon farms in the marine environment (Bravo

et al. 2020; Cvitanich, Garate, and Smith 1991). Survival of *P. salmonis* inside cells in seawater for periods of greater than 14 days is possible under cold water conditions (< 10°C) (Lannan and Fryer 1993). It is possible that extended survival of bacterial pathogens in sea water could occur, given the genetic similarities between NZ-RLO pathogens and *P. salmonis*.

Hydrodynamic connectivity has been shown to be important in estimating bacterial spread between farms (Bravo et al. 2020). To estimate connectivity, an understanding of water transport is required, which was estimated here using results from an existing high-resolution hydrodynamic SCHISM model (Zhang et al. 2016). Coastal currents were available from an unstructured hydrodynamic model, which was constructed for the Marlborough Sounds and wider region (Figure 3) and covered a period from 2008 to 2017. Model validation was performed on 11 in situ current meters from throughout the Marlborough Sounds and showed good reproduction of the magnitude and phase of tidal flows, residual flows and elevations throughout the region (MSL 2019). Given the tidal dominance of the currents in the region investigated in this study, the model was deemed suitable for the purposes of estimating general connectivity between the sites.

Pathogen connectivity and travel times between four farm sites, all located in Pelorus Sound, were simulated from the hydrodynamic model data using the OceanTracker software developed by Vennell et al. (2021). This approach uses Lagrangian particle tracking and a controlled continuous release of passive particles from the defined salmon farm site in the hydrodynamic domain. Passive particles (i.e., neutrally buoyant particles with no behaviour) were tracked in three-dimensions in the simulations with released particles counted as they entered other receiving farm sites, in a similar manner to Bravo et al. (2020).

To generate information on connection probabilities and time-of-travel throughout the model domain, all salmon farm locations were simulated with both specific release and receiving locations defined based on salmon farm area polygons. Vertical dimensions were also included and cover the water depth from the surface of the farm site to 15 m deep (i.e., the depth of the salmon net pens). Polygon information for all operating salmon farms was obtained from aquaculture licence information provided by the New Zealand Ministry for Primary Industries (MPI) (MPI 2021).

Connectivity was estimated from Lagrangian tracking of individual particles in the OceanTracker software, with particle age information (the time since the particle was released) also recorded. The particles were continuously released from each source polygon at a rate of 200 per release region per particle tracking time step (10 min) over a 90-day release period, from 1 December 2010 to 29 February 2011. In total, 10,368,000 particles were released across the four farm sites over the duration of the simulation. The 2010/2011 period was selected, because it was associated with similar La Niña conditions to those experienced over the 2021/2022 mortality event, although tidal currents provide the dominant driver of flows in the area.

Connectivity was calculated from the number of particle arrivals at each site and each daily age band, divided by the total

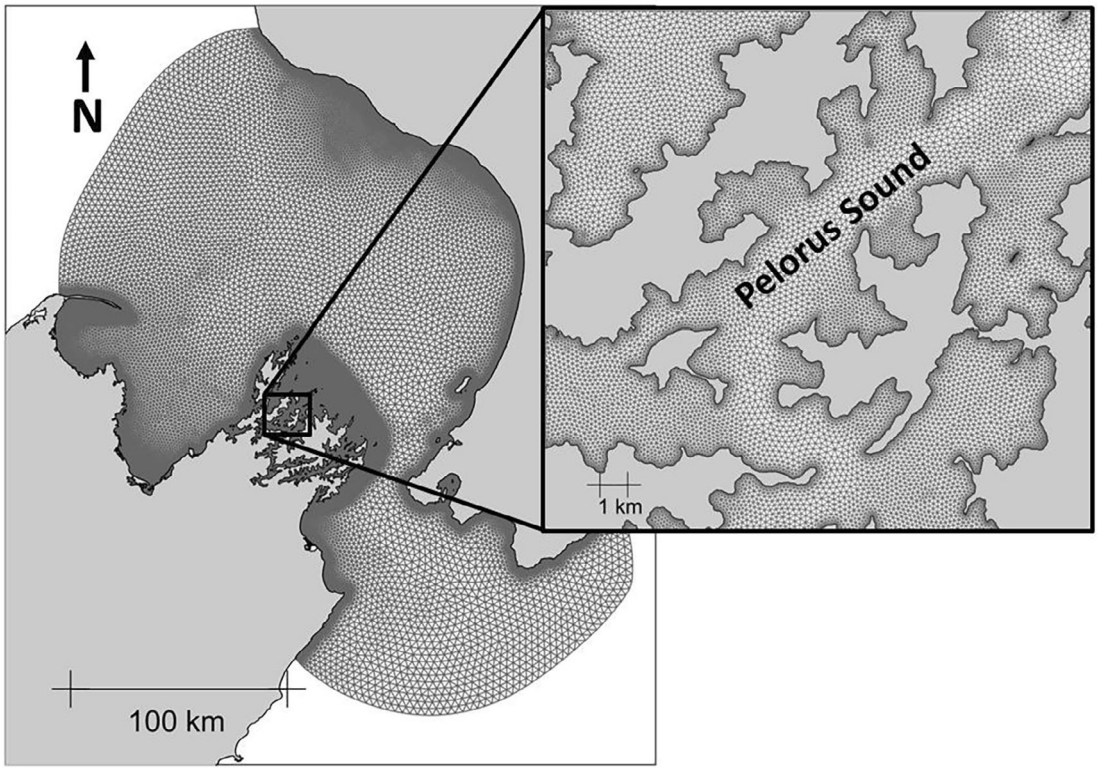

FIGURE 3 | Hydrodynamic model domain and triangular mesh (grey triangles). Images show the domain encompassing Cook Strait and the waters around central New Zealand (left) and Pelorus Sound region where this study was conducted (right). The highest grid resolution is about 20 m near to the coast.

number of arrival events that were possible based on the released particles in each daily age band and the number of times the particle locations were checked (i.e., the model time step). This produced an adjacency matrix (λ) of undecayed connection probabilities between the source and destination locations for each age grouping of the particles.

Pathogen decay (determined from a time to 90% loss and defined as T_{90}) is an unknown parameter in the simulations; therefore, a decay-adjusted connectivity (λ^*) was also calculated for each simulation. Decay was calculated *post hoc* during the SIR modelling process, as described below.

3.2 | Decay-Adjusted Connectivity and Calculation of Time-Of-Travel

Decay-adjustments for connectivity (λ^*) were calculated based on nondecayed connectivity (λ), and T_{90} decay, for all particle ages (τ), as follows:

$$\lambda^* = \lambda\, e^{-k\,\tau} \tag{1}$$

$$\text{where } k = \log_e(0.1) / T_{90} \tag{2}$$

Total connectivity (Λ), across all ages (a) and between all sites (i, j), was calculated as:

$$\Lambda^*_{i,j} = \sum_{a=1}^{A} \left(\lambda^*_{i,j,a}\right) \tag{3}$$

where A is the maximum age (in days) and with:

$\Lambda^*_{i,j} = 1$, where $i = j$ to ensure complete connectivity was applied within SIR populations at each site.

The mean time-of-travel between sites was also affected by pathogen decay, with the time-of-travel between sites (τ^*) was calculated based on connectivity-weighted particle delay between each pair of sites. This calculation was made for each connection, based on the age (a), decay-adjusted connectivity (λ^*) and total connectivity (Λ) as:

$$\tau^*_{i,j} = \frac{\sum_{a=1}^{A} \left(\lambda^*_{i,j,a} \cdot a\right)}{\Lambda^*_{i,j}} \tag{4}$$

and with:

$\tau^*_{i,j} = 0$ where $i = j$ to ensure no delays were applied within a site. This equation shows that decay reduces the number of older particles arriving at the site, which lowers the total connectivity and the mean age of particles (i.e., the time-of-travel) moving between a pair of sites.

3.3 | Susceptible, Infected, and Recovered (SIR) Modelling

After calculating decay-adjusted pathogen connectivity and time-of-travel between sites, a delay-differential dynamic SIR modelling approach was used to investigate disease progression within each salmon farm site in Pelorus Sound. Ideally, an existing open SIR modelling framework would have been used for our study, such as the recently developed open-source DTU-DADS-Aqua framework for the infectious salmon anaemia virus (ISAV) (Romero et al. 2021), or the 'hybridModels' framework (Marques et al. 2020). However, there were limitations in the use of both of those frameworks, such as a lack of recovered population to account for vaccine use in the DTU-DADS-Aqua framework and a lack of accounting for travel time delays in the simulation of infection spread in both frameworks. Consequently, a customised modelling approach was developed for this study. We used an ensemble parameter search approach to estimate plausible parameterisations to simulate observed industry-supplied mortality data from the 2022 mortality event in Pelorus Sound.

Key to providing a useful model for the region is the ability to simulate the timing and magnitude of mortality and estimate potential drivers. Potential drivers include the following: residual pathogen loads, infection pressure from nearby farms and wildlife, differential environmental and other site-specific stresses from the individual farm sites. Where possible, the model parameter ranges are informed from available information for NZ-RLO, or *P. salmonis*, (see Section 3.5). Given the limited information available to parameterise a detailed model, and to reduce complexity, the model has been designed to be relatively simple, with parameters restricted to the minimum required for effective simulation of the event (Figure 4).

The recovered (R) population in the SIR model can also be used to simulate vaccinated individuals in the population that may be resistant to infection for a given period. Simulating vaccinated individuals was important for the case considered here and provided some additional flexibility that was not present in other modelling frameworks (e.g., Wada et al. 2021; Romero et al. 2021).

The underlying dynamic SIR model developed for this study is based on the SIR modelling equations detailed in Anderson and May (1979). However, the equations have been extended to incorporate hydrodynamic connectivity and the potential for transmission of infection between farm sites.

The underlying differential equations for the susceptible (S_i), infected (I_i) and recovered (R_i) populations for a given site, i are defined as:

$$\frac{dS_i}{dt} = \gamma R_i - m_{nml} S_i - \beta^* S_i \sum_{j=1}^{n} \left(I_{i,j,t-\tau}\, \Lambda^*_{i,j,}\right) \tag{5}$$

$$\frac{dI_i}{dt} = \beta^* S_i \sum_{j=1}^{n} \left(I_{i,j,t-\tau}\, \lambda^*_{i,j}\right) - \left(m_{nml} + m_{inf} + \nu\right) I_i \tag{6}$$

$$\frac{dR_i}{dt} = \nu\, I_i - \left(\gamma + m_{nml}\right) R_i \tag{7}$$

The parameter β refers to a pathogen transmission coefficient and is used to define the rate of transmission from infected to

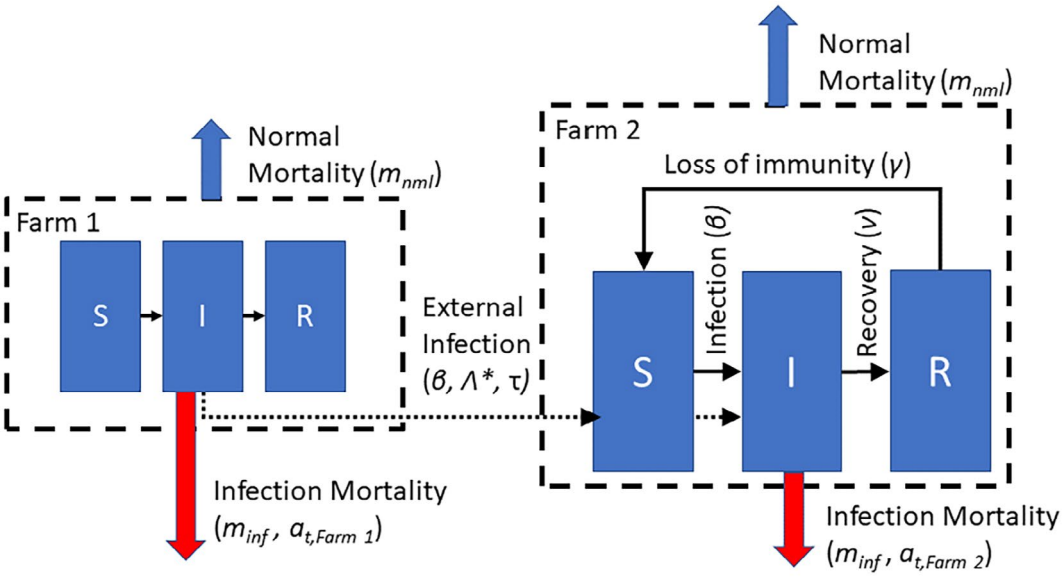

FIGURE 4 | Schematic of a dynamic model for two farms, showing key susceptible (S), infected (I) and recovered (R) populations simulated within each farm, as well as infection transfer between farms (external infection), normal (whole population) mortality, and infected mortality. Symbols in parentheses refer to key model parameters which affect the associated population categorisation flows (see Section 3.5).

susceptible individuals within a site (Anderson and May 1979). In the context of this model, β was also extended to include the infection pressure from external infected sites connected to receiving susceptible populations and is referred to here as β^* to clarify the difference from the typical use of this term.

The parameter $\Lambda^*_{i,j}$, refers to a matrix of decay-adjusted hydrodynamic connectivity probabilities between all sites (i,j) and all particle ages (i.e., the probability that a viable pathogen propagule of any age arrives at farm i from a distant farm site j). This connectivity is precalculated from the particle tracking modelling based on the selected decay parameterisation, as discussed in Section 3.1.

The infected population $I_{t\text{-}\tau}$ refers to the delayed state of infected populations at all farm sites hydrodynamically connected to site i (where a delay, τ, is specific to each site pairing—see following connectivity modelling section). Infections from an infected farm can spread to an uninfected farm, or enhance the infection rates at distant farms with existing infected populations, if the pairwise connectivity is nonzero (i.e., $\Lambda^*_{i,j} > 0$). Model calculations from external farms are made based on the historical infection state of connected farms (i.e., current time minus any time-of-travel delay).

The parameter ν in Equations (6) and (7) defines the rate of recovery from infection, and γ defines the loss of immunity rate for the recovered populations.

The parameters m_{nml} and m_{inf} refer to the normal and infected mortality rates, respectively, with a mortality modifier ($a_{t,i}$) used to modify the infected mortality rates through time (e.g., due to increased temperature stress) and for each location. All parameter rates used in the model were defined at a weekly scale.

For the purposes of this study, most parameters (i.e., β^*, T_{90}, m_{nml} and m_{inf}) were set to be equal across all farms for each simulation. The exceptions were the pairwise connectivity (λ) and the time-of-travel delays (τ), which were calculated and defined for each combination of sites based on particle tracking results. The pairwise connectivity and the time-of-travel delays are provided in the form of adjacency matrices. The mortality modifier ($a_{t,i}$) was also different for each farm, to account for differences in observed mortality between sites. This was important in determining site-specific mortality and needed to be included to ensure infection mortality could vary between sites. The calculation of this parameter is discussed in the following section.

3.4 | Assessing Temperature- and Farm-Linked Infection Mortality

Weekly mortality counts were collected by farm staff and provided for this study by the farm managers. These mortality data provided suitable information to quantitively assess the model performance, with mortality differences between sites seen in the 2022 event (Figure 2). These data show that the 2021/2022 Pelorus Sound mortality event was the largest observed in the region following two decades of salmon farming and that mortality was highly variable between the farm sites (see Section 2).

Multiple factors likely contributed to the observed mortality and the differences between sites, and that coincident increase in the timing in the growth of the cumulative mortality imply that temperature-linked drivers of mortality were likely important during the 2022 event. Quantitative data on animal stress were not available to parameterise a complex mechanistic approach to modelling a potential cause of the observed mortality differences. However, various site differences may have had an impact on fish mortality, with potentially important factors including water temperature, water current speeds, presence of predators (e.g., seals), concentrations of free-floating pathogenic material (i.e., NZ-RLO1 and *T. maritimum*) or differences in husbandry practices (e.g., differences in net cleaning frequency and upwelling bubbler use).

To reduce the complexity, a single farm-specific mortality modifier ($a_{t,i}$) for infected fish was applied to each site (i) to simulate observed differences in mortality rates at different temperatures (t). The farm-specific mortality modifier ($a_{t,i}$) is based on the product of a temperature-specific modifier (a_t) and a site-specific modifier (a_i), such that:

$$a_{t,i} = a_t a_i.$$

To investigate how the inclusion of temperature-linked and site-specific drivers affected model outcomes, five candidate scenarios were tested (Table 1).

To ensure consistency with observations of low mortalities at low temperatures, a minimum critical temperature (T_c) was set. Below this critical temperature, it was assumed that no infection mortality was present ($a_{t,i}=0$). This critical temperature was set to be 17°C, based on observations of low mortalities below this temperature and for the purposes of the model below which additional infection mortality was assumed to be zero. However, because 'normal' mortality was modelled as constant across all temperatures and may be associated with pathogens, low-temperature (i.e., below 17°C) mortalities could still be reproduced by the model. As with the infection mortality parameter, the normal mortality parameter rate was also varied for each simulation to help find the best fit to the measured mortality data.

For all linear and quadratic infection mortality scenarios, estimated minimum critical (T_c), and standard (T_s), temperatures were used to simulate a ramp up in thermal-linked mortality. The standard temperature was set to 18°C, a level at which the site-specific infected mortality (m_{inf}) was unmodified by temperature (i.e., $a_{t,i}=1$ at 18°C). The variation in mortality was determined from temperatures ($T(t)$) recorded in the region and any site-specific modifiers (a_i). Specifically, the calculations for the linear (8a) and quadratic (8b) mortality modifying equations were as follows:

$$a_{t,i} = \left[a_i \cdot \left(T(t) - T_c\right) / \left(T_s - T_c\right)\right] \qquad T(t) > T_c \qquad (8a)$$

$$a_{t,i} = \left[a_i \left(T(t) - T_c\right) / \left(T_s - T_c\right)\right]^2 \qquad T(t) > T_c \qquad (8b)$$

and with

$$a_{t,i} = 0 \qquad T(t) < T_c \qquad (8c)$$

In the case of Scenarios 1 to 3, site-specific modifiers (a_i) were set to one for all sites. In the case of Scenario 4 (linear temperature-linked mortality), the a_i values for each farm were calculated as the maximum observed weekly mortality rate divided by the farm with the lowest observed mortality, at the standard temperature (Table 2). In the case of Scenario 5 (quadratic temperature-linked mortality), the site-specific mortality modifier values (a_i) values for each farm were assessed based on the square root of the Scenario 4 values (Table 2).

This approach was used in our simulations because infection mortalities were observed to be much larger than normal mortality during periods of elevated water temperatures. However, this approach would need to be refined if other sources of mortality were determined to be similar, or dominant, to infection mortality rates.

3.4.1 | Numerical Integration and Sensitivity Analysis

The integration of the differential Equations (5–7) was undertaken using a 4th–5th order Runge–Kutta numerical scheme with time-adaptation to limit numerical errors. The numerical experiments were conducted in the Julia programming language (Bezanson et al. 2017) by applying the TSit5 algorithm (Tsitouras 2011) with a default parameterisation from the Differentialequations.jl package (Rackauckas and Nie 2017). The nominal output time step used by the model was a week, but internal time adaptive solving, means that the internal integration time steps may be smaller than this to meet solver tolerance criteria. A copy of the Julia code used to undertake the simulations can be provided upon request.

3.5 | Model Parameterisation and Performance Assessment

Even with the relatively simple dynamic model developed for this study, several potential influential, and uncertain, model

TABLE 1 | Scenarios used to investigate the effect of temperature and farm-specific effects on mortality.

Scenario	Description	Farm-specific mortality modifier ($a_{t,i}$)
1	No site or temperature-linked mortality modification	$a_{t,i}=1$
2	Linear temperature-linked mortality modification, same across all sites	$a_t \propto$ temperature, $a_i=1$
3	Quadratic temperature-linked mortality modification, same across all sites	$a_t \propto$ temperature^2, $a_i=1$
4	Linear temperature-linked mortality modification, varying across sites	$a_{t,i} \propto$ temperature
5	Quadratic temperature-linked mortality modification, varying across sites	$a_{t,i} \propto$ (temperature × site)^2

parameters exist. Consequently, model tuning of the six parameters present was conducted using ensemble simulations to explore the importance of model drivers of infection.

There is a paucity of information for combinations of pathogens and affected host species, so a common approach is to use information from similar systems with similar pathogens and affected species (e.g., Romero et al. 2021). Limited epidemiological information is available on bacterial infections of Chinook salmon, although some studies are available for *P. salmonis* (e.g., Cvitanich, Garate, and Smith 1991), with most research undertaken on Atlantic salmon, *Salmo salar*. Where possible, relevant information from a model bacterium, *P. salmonis*, were used as a primary resource to determine parameter range values for the epidemiological model developed here. Chilean studies contain a significant amount of information on *P. salmonis* growth rates, seasonality and persistence (i.e., survival time outside of a host) (Bravo et al. 2020; Cvitanich, Garate, and Smith 1991; Lannan and Fryer 1993; Olivares and Marshall 2010). While there are similarities between NZ-RLOs and *P. salmonis*, our aim was to develop a general bacterial model rather than a NZ-RLO-specific model given evidence of concurrent *Tenacibaculum* species infection (Table 5).

Ensemble simulations were configured to simulate the period from 1 October 2021 and were run for a period of 30 weeks, using literature-sourced and estimated values ranges for the six model parameters (Table 3). Although *P. salmonis* was used as the model bacterium for our simulations, overlap with other bacterial pathogens are possible for some parameters. For example, a pathogen decay time spanning 0–10 days covers the 5-day survival period for *T. maritimum* in nonsterile seawater observed by Avendaño-Herrera, Toranzo, and Magariños (2006).

A sample size of 4096 simulations using parameters determined from quasirandom number distributions were precalculated to ensure even coverage of the parameter space, rapid calculation and low cross-correlation between parameters. The quasirandom number distributions were constructed using the Sensobol package (Puy et al. 2022) in the R programming language (R Core Team 2024) using a first-order effects sampling strategy (Saltelli et al. 2008). Larger numbers of simulations, up to 61,440, were also conducted to improve the sampling of the parameter resolution and determine whether the parameter selection could be further optimised.

The performance of each simulation was assessed based on their ability to reproduce total observed mortality (i.e., infection and other mortality) across all the farm sites. Model performance was calculated from the root-mean-squared error (RMSE) between modelled total mortality and measured total mortality for each simulated week and farm site. To prevent over assessment of the model performance during the early period of the simulations when mortality at all farms was at, or close to, zero, the first 10 weeks of the simulation (i.e., up to December 2021) were excluded from the calculation of RMSE. The summed RMSE value of all times and individual farm sites was used to determine the best performing parameterisation, with the lowest value indicating the best performance.

3.6 | Initial Conditions

The model was initialised so that fish totals for each farm were equal to production estimates of in situ fish counts (Table 4). It was assumed that very low levels of infection (1 fish per 1000) existed at all farms at the start of the simulation, given no detection of NZ-RLO1-infected fish until January 2022 from targeted sampling of at least five moribund fish per farm site in each month (Table 5).

Inactivated vaccine developed specifically for NZ-RLO 1 and *T. maritimum* isolated from chinook salmon in New Zealand

TABLE 2 | Mortality modifiers used in the linear and quadratic scenarios where site-specific variation was applied.

Farm site	Linear mortality modifier	Quadratic mortality modifier
Kopaua	2.42	1.56
Forsyth	1.79	1.34
Waihinau	7.02	2.65
Waitata	1	1

TABLE 3 | Model parameter ranges used in the ensemble simulations.

Parameter	Short name	Symbol	Value range	Rationale/Reference
Transmission coefficient	beta	β^*	1×10^{-7}–1×10^{-6}/week	Maximum value set to ensure model stability
Normal mortality	mortn	m_{nml}	0%–1%/week	Maximum estimated from mean weekly mortality of 5 years (2017–2022) of historic industry data
Infected mortality	morti	m_{inf}	0%–6.17%/week	Maximum from Bravo et al. (2020)
Loss of immunity	lossim	γ	0%–4%/week	Estimated assuming a minimum of 4 months of 50% immunity
Recovery rate	recov	ν	0%–1%/week	Estimated by assuming that up to 1 in 100 fish recover from infection per week
Pathogen 90% decay time	decayt90	T_{90}	0–10 days	Lannan and Fryer (1993)

was administered to 80% of hatchery fish that were subsequently stocked at Waitata only. This vaccine has been shown to provide some protective effect against NZ-RLO1 via intraperitoneal challenge (Jaramillo et al. 2023); however, with a moderate relative percent survival (RPS = 48.8%), it only offers limited protection. The vaccine provided no protective benefit in NZ-RLO1 immersion challenges; and given low (< 20%) mortality was noted in immersion control fish, limited conclusions could be drawn from the study (Jaramillo et al. 2023). For our simulations, we assumed 50% efficacy of the vaccine. Consequently, only 40% of the fish at the Waitata site were estimated to be effectively vaccinated and initialised as part of the recovered population in the model (i.e., 80% vaccination × 50% efficacy = 40% protected) (Table 4).

Disease surveillance was conducted through monitoring five, or more, moribund fish per farm per month between October 2021 and May 2022 (i.e., less than 0.001% of the fish at each of the sites but was targeted at moribund animals; Table 5). Up to 10 fish per farm were sampled in the worst-affected farms during the height of the mortality event. In brief, fish were tested for the presence of NZ-RLO1 using a species-specific polymerase chain reaction (PCR) test from samples taken from internal organs (pooled anterior kidney, liver and spleen) and/or from the edge of skin lesions. The presence of NZ-RLO1 and its association with disease was further supported by histopathology interpretation from internal organs made by the Ministry for Primary Industries, although the potential for other viral or bacterial agents could not be completely ruled out (data not shown). Surveillance for *Tenacibaculum* spp. involved the use of skin swabs inoculated on selective media and observed colony growth in association with gross clinical disease (i.e., skin lesions; Kumanan et al. 2022). In this study, pathogen detection was considered binary (either detected or nondetected) for a given sampling event (Table 4).

Inactivated bivalent vaccine developed specifically for NZ-RLO1 and *T. maritimum* isolated from king salmon in New Zealand was administered to hatchery fish that were subsequently

TABLE 4 | Initial susceptible, infected, and recovered population sizes used to initialise the model simulations.

Farm site	Short name	Susceptible	Infected	Recovered	Total
Kopaua	KOP	316,125	316	0	316,441
Forsyth	FOR	541,677	542	0	542,219
Waihinau	WHN	681,857	683	0	682,540
Waitata	WAT	393,188	656	262,563	656,407

Note: High numbers of recovered fish at the Waitata site were used to simulate vaccinated fish with 40% of the fish assumed to be resistant to infection (i.e., recovered).

TABLE 5 | Pathogen surveillance results of moribund fish.

		Month (Weeks)							
		Oct-21	Nov-21	Dec-21	Jan-22	Feb-22	Mar-22	Apr-22	May-22
Pathogen	Site	(0–3)	(4–8)	(9–12)	(13–16)	(17–20)	(21–24)	(25–28)	(29–32)
NZ-RLO1	KOP	ND	ND	ND	ND	D	D		
	FOR	ND	ND			D			ND
	WTA	D+	ND	ND	ND	D+	D+		D+
	WHN	ND			D			D	
Tenaci. spp.	KOP			D TM, TD		D TM, TS, TD	D TM, TD		
	FOR	D TD, TM				D TM			D (PCR) TM
	WTA	D TD		D TM	D TM, TD	D TM	D TM, TD		D TD
	WHN	D TM			D TM, TD			D TM	

Note: Detection (D) and non-detection (ND) of NZ Rickettsia-like organism (NZ-RLO1) and Tenacibaculum species (*Tenaci.* spp.) are shown from Pelorus farm sites, with positive detections indicated with grey shading.
Abbreviations: D+ is used to indicate NZ-RLO 1 polymerase chain reaction detection on fish at the Waitata site, and is not shaded grey as it could represent false positives through cross-reactivity with inactivated vaccine. KOP = Kopaua, FOR = Forsyth, WTA = Waitata and WHN = Waihinau. Blank cells indicate that no fish were sampled. TM = *T. maritimum*, TS = *T. soleae* and TD = *T. dicentrarchi* detection.

stocked at Waitata only. Consequently, it is possible that NZ-RLO1 false-positive PCR results could occur from Waitata fish post administration of the vaccine, given known cross-reactivity (data not shown). NZ-RLO1 PCR detection from Kopaua, Forsyth and Wahinau, which were not vaccinated with the bivalent vaccine, was considered true positives.

3.7 | Vaccine Performance Assessment

The performance of the vaccine was also assessed by repeating simulations using the parameters from the best simulation, but with the initial recovered fish populations altered to reflect the vaccine strategy being investigated. The total cumulative mortality at each site was then used to assess the performance of two vaccination strategies against a no-vaccination scenario.

The first vaccination strategy was the scenario used to validate the model (i.e., only Waitata). A second vaccination strategy also considered a scenario where the same amount of vaccine applied in the 2021/2022 event was applied to the worst impacted farm site (Waihinau), instead of the Waitata farm. This was to investigate whether an alternative farm stocking choice could have affected the effectiveness of the vaccination programme. Again, this alternative vaccine scenario was rerun using the same model parameters from the best performing simulation.

4 | Results

Understanding connectivity and time-of-travel between the farms formed an important aspect of the networking component of the model, allowing infection pressure from nearby farms to contribute to disease progression in nearby farms. The result of this work suggests that despite the proximity of the farms and strong currents, that connections were relatively weak. Only about 2% of simulated particles passed between the most connected sites, Waihinau and Waitata, and only about two in one thousand particles (0.2%) passed between the more distant farms when no decay was present (Figure 5).

The weighted-mean connection age of particles (used to estimate pathogen decay and model delays) was also quite long, with a minimum connection time of about 6 days for close sites (i.e., between Waihinau and Waitata), but up to 15 days estimated for more distant sites (e.g., Forsyth and Waitata; Figure 5). There was a general pattern of shorter time-of-travel being associated with higher connectivity and some asymmetry between farms was also visible in the connectivity and time of travel results.

4.1 | Mortality Modelling

The model showed a strong response to the inclusion of temperature-linked and site-specific mortality adjustment, with a poor comparison to observations noted for the best performing

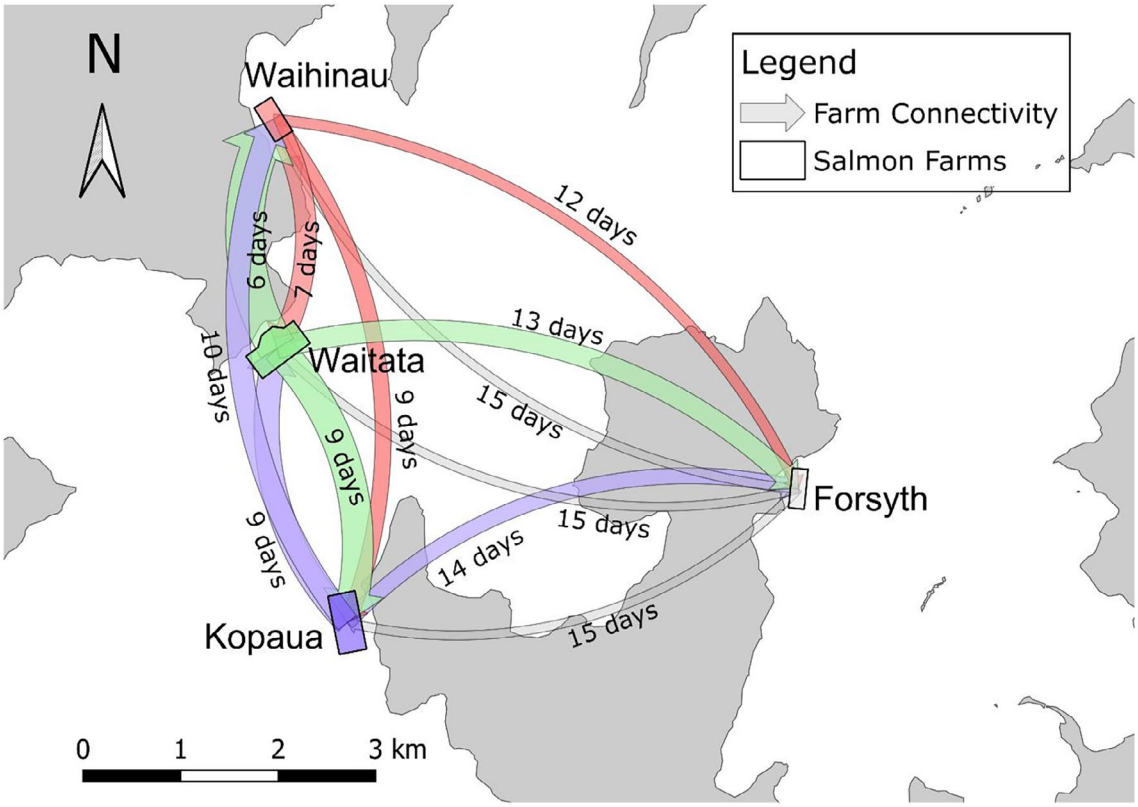

FIGURE 5 | Map of undecayed connection strengths and travel times between salmon farm sites in the outer Pelorus Sound, with the farm colour matching the outward arrow colour. Arrow width is proportional to connectivity strength, and the travel times shown relate to the connectivity-weighted average age of the particles passing between the sites. The highest connectivity was between Waihinau and Waitata (2.9% of particles released from Waitata reached Waihinau) and had a travel time of 6 days. The least connected farm site was Forsyth to Waihinau, with less than 0.2% connectivity and a time-of-travel greater than 2 weeks from Forsyth to all other farm sites.

constant infection mortality model (i.e., Scenario 1; see Table 1). Modelling temperature effects without site-specific differences (i.e., Scenarios 2 and 3; Table 1) showed an improvement in the model performance. However, peak mortality at the worst-affected farm site, Waihinau, was substantially underestimated when temperature and site-specific effects were not included. Consequently, both site-specific and temperature-modified mortality was required to recreate the observed mortalities (i.e., Scenarios 4 and 5; Table 1). Of all approaches considered, the quadratic temperature approach (i.e., Scenario 5) showed the lowest total RMSE value and was used in all subsequent simulations.

Considering the total RMSE ($RMSE_{tot}$) across all sites for the best performing simulation shows that adding only temperature mortality modifications reduced the $RMSE_{tot}$ by about 4% (i.e., improved the performance). Whereas the $RMSE_{tot}$ was reduced by about 46% when both site-specific and quadratic temperature modifications were included. These results support the importance of including both the combination of site-specific factors and quadratic temperature effects in this event.

Comparison of the best performing scenario's ensemble predictions of mortality showed a wide variety in model performance to measured data. The best performing model result had a mean relative RMSE across all sites of 8.3%, defined as 'excellent' performance (i.e., $<10\%$) (Jamieson, Porter, and Wilson 1991; Li et al. 2013; Despotovic et al. 2016). Inspection of the best result shows that the model was able to approximate the magnitude and timing of growth and decay of the mortality event well across three sites, including the worst-affected Waihinau (WHN) site (Figure 6). However, the model underestimated observed peak weekly mortality at the Kopaua site (KOP) by about 50% (Figure 6).

Examination of the minimum and maximum range of results from the best 2% of model simulations indicate a wide variation in performance when compared to measured mortality. For example, it appears that some simulations could better predict the maximum mortality at the worst-affected Waihinau site (Figure 6). However, such simulations also overestimated mortality at Kopaua, so performed worse overall.

4.2 | Wider Simulation Performance and Inferred Parameter Ranges

Despite differences in the modelled ensemble results, inspection of parameters for the best simulations, with 2% lowest RMSE values (i.e., 82 simulation values), highlight some commonalities in the parameter values (Figure 7). Specifically, the transmission coefficient (beta), decay time (decayt90), infection mortality (mrti) and the loss of immunity (lossim) and recovery (recov) rates were observed to cover a narrower range of values in the best performing simulations (Figure 7). The best performing simulation was generally consistent with the best 2% of simulations for most parameters (Figure 7). However, the main exceptions were the recovery rate (recov) and mortality rates (mrti and mrtn), which were at the low and high end of the ranges, respectively (Figure 7).

The presented results have not been optimised to select the parameters. However, increasing the resolution of the parameter search space by increasing simulations by up to 15 times (i.e., to 61,440) showed a reduced performance, with an increase in the RMSE of 70% in the largest ensemble. This was an unusual result but highlights local optima likely occupy a small area of the parameter hyperspace and that our parameter results were likely near optimal at the level of simulations employed (i.e., 4096 simulations). Further optimisation is likely

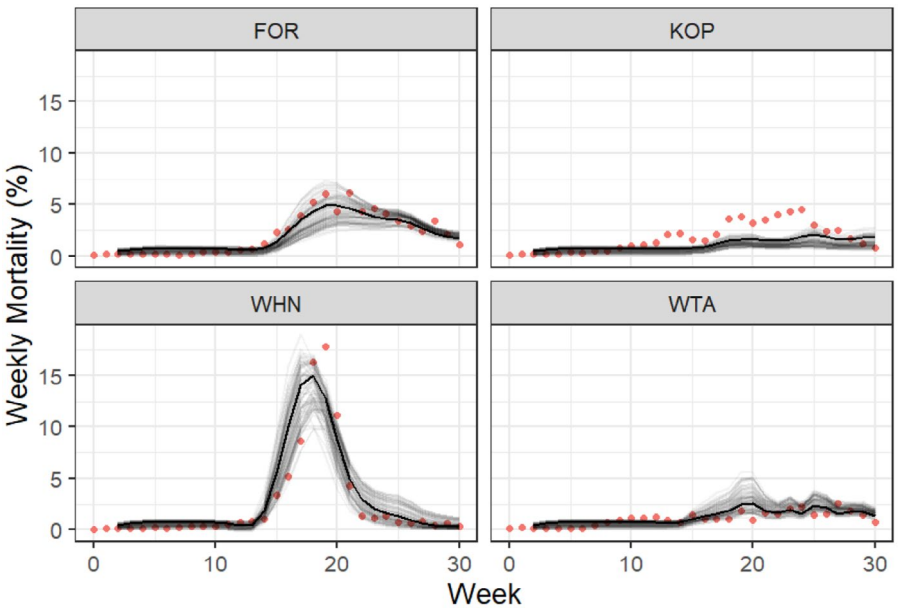

FIGURE 6 | Best performing modelled weekly mortality result (black line) compared to data (red circles) from the simulation using a linear temperature-linked and site-specific mortality modifications. The best 2% of simulations are shown as a grey lines. Farm abbreviations are FOR = Forsyth, KOP = Kopaua, WHN = Waihinau and WTA = Waitata.

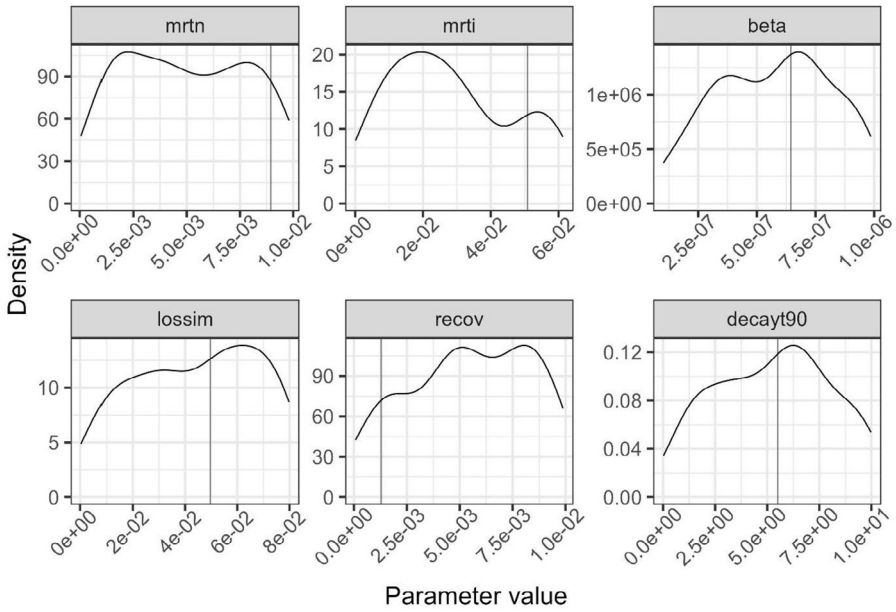

FIGURE 7 | Density of parameters from the best 2% performing model simulations, relating to the lowest total root mean squared residual error across the four farm sites. Vertical lines indicate the parameter values for the best performing simulation. Parameter abbreviations on the figure are: Transmission coefficient = beta, normal mortality = mrtn, infected mortality = mrti, loss of immunity = lossim, recovery rate = recov, pathogen 90% decay time = decayt90.

possible, but this was not a focus of this study and the best parameter results seem plausible, with agreement between the best performing simulations and estimates from studies on *Piscirickketsia salmonis*.

A decay time (decayt90) for the best performing simulation was around 5 days, which was consistent with the detections of *P. salmonis* after 7 days at 20°C in the study of Lannan and Fryer (1993). Our result was also consistent with the 5-day survival period for *T. maritimum* in nonsterile seawater observed by Avendaño-Herrera, Toranzo, and Magariños (2006), although one would expect a lower survival time in the unsterilised seawater of Pelorus Sound. The best estimate for the loss of immunity rate (lossim) was around 4%–5% per week (i.e., a 50% loss of immunity over about 14 weeks/3.5 months), which is lower than other reported vaccine efficacy periods for *P. salmonis* (e.g., 8 months—Wilhelm et al. 2006; 10 months—Salonius et al. 2005). The recovery rate in the best simulation also appeared to be low, at around 0.1% per week, suggesting few infected fish would survive to become resistant.

4.3 | Estimation of Latent Disease Dynamics

A key goal of the study was to formulate working hypotheses on the potential rate of infection growth that may have occurred prior to the mortality event. This was to help inform the speed of response required for management actions in future. Inspection of the best performing model simulations show the modelled change in the proportion of infected individuals at the sites. This result shows rapid infection of the susceptible farm populations of salmon, with growth from low infection (< 10%) to near full infection (> 90%) at the sites estimated to take approximately 5 weeks (with the exception of Kopaua and the vaccinated Waitata site) (Figure 8).

4.4 | Estimated Performance of Vaccine

Based on consideration of a scenario where no vaccination occurred, it appears that about 10% fish were protected by the application of the vaccine to the Waitata site (Table 6). However, if the fish in the worst-affected Waihinau farm site were vaccinated instead of the Waitata site, our simulations suggest that almost 20% of the fish that died in the unvaccinated scenario could have been protected (Table 6).

5 | Discussion

The SIR disease model trained on mortality data from a Chinook salmon mortality event in Pelorus Sound, New Zealand, was able to reproduce observed mortality across three of the four salmon farms. Relationships between the model parameters and model estimates of mortality are complex, but we show that values of key parameters including decay time, infection mortality, loss of immunity and recovery rates, from the best performing simulation appear to be consistent with other bacterial pathogen studies. For instance, studies conducted for *Piscirickettsia salmonis* on Atlantic salmon, and on the survival of *T. maritimum* in seawater. However, limited data on infection progression for candidate pathogens (Table 5), meant that robust validation of infection dynamics was not possible in this study. Nevertheless, it appears that the simulations were able to reproduce observed mortality patterns at most farms, with the exception of the Kopaua farm where mortality was underestimated by the model.

Measured peak mortality at the Waihinau site occurred at around Week 20, approximately 5 weeks after the best-fitting model predicted peak infection at the site (Figure 6). Similarly, simulated infection levels at Waihinau of greater than 50% prevalence occurred around Week 11 (Figure 8), approximately 5 weeks earlier than

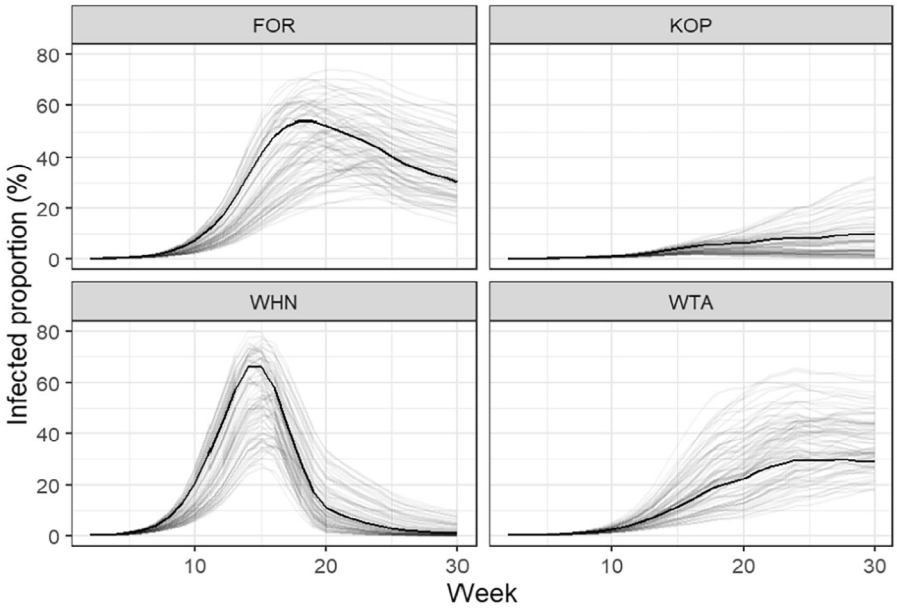

FIGURE 8 | Modelled proportion of the population infected at all sites for the best simulation (solid black line). The best 2% of simulations are shown as grey lines. NZ-RLO surveillance at the worst-affected Waihinau site occurred during Weeks 4, 16 and 28, with detection of the disease (in all sampled fish) in Week 16 (not shown here—see Table 5). Peak mortality at the site occurred around week 20 (February 2022) of the simulation (see Figure 6). Farm abbreviations are FOR = Forsyth, KOP = Kopaua, WHN = Waihinau and WTA = Waitata.

TABLE 6 | Comparison of total mortality outcomes for each farm site from three vaccination scenarios, with no vaccination (No vacc.), only the Waitata farm (WTA vacc.) or only the Waihinau farm (WHN vacc.) vaccinated.

Scenario	KOP	FOR	WHN	WTA	Total mortality	Mortality difference	% Difference
No vacc.	107,384	334,303	621,935	402,641	1,466,262	0	0.0%
WTA vacc.	107,529	335,338	622,199	247,838	1,312,904	-153,358	−10.5%
WHN vacc.	107,623	334,677	329,142	404,544	1,175,986	-290,277	−19.8%

Note: Differences shown as reduction in total mortality from the 'No vacc.' Scenario and the 'WTA vacc.' scenario summarising the modelled cumulative mortality from Figure 6.
Abbreviations: (farm) FOR = Forsyth, KOP = Kopaua, WHN = Waihinau and WTA = Waitata.

detection of the pathogen in moribund fish occurred. However, small monthly sample sizes (i.e., 5–15 moribund fish were sampled per site) does not lend itself to model validation of infection prevalence. Nevertheless, sampling of moribund fish is valuable to determine pathogens most likely associated with mortalities, and such data were still extremely valuable in retrospectively attributing likely pathogenic drivers of the event. Surveillance data will also be more likely to be valuable in future following validation of test sensitivity (Jaramillo et al. 2023) and population-based/environmental monitoring to determine whether pathogens can be detected earlier in the disease cycle. Moreover, where inactivated vaccines are administered in future, it would be prudent to use a viability PCR where only the DNA (or RNA) of live cells will be detected.

Should high infectivity be proven, as implied the results of this modelling study, alternative strategies to reduce infection pressure could also be considered. For example, early culling/emergency harvest of infected fish could be used, should a lack of access to effective vaccinations not be possible in future. In addition, periods of fallowing are also recommended as an approach to limit the spread of *P. salmonis* (see Olivares and Marshall 2010). Fallowing is not routinely applied in the Marlborough region, but can be used in response to detection of poor benthic conditions at salmon farms. Similarly, 'firebreak' strategies, where managed spacing between farms can be used to prevent spread, have also been suggested for other marine pathogens (Salama and Murray 2013) and parasites (Samsing et al. 2017). The Pelorus Sound farms considered here were all in relatively close proximity (i.e., < 5 km apart; Figure 1), so thought could be given to trying to reduce the impact of this proximity in future.

5.1 | Infection Dynamics and the Relative Roles of Candidate Pathogens

Our theoretical modelling indicates that the progression of disease may occur quite quickly, but that associated fish deaths may occur a long time after initial infection (i.e., more than a month). However, coincident increase in temperature also coincided with peak mortality, which suggests multiple factors likely

contributed to the high observed mortality at the site. Given that the observed patterns in mortality could not be resolved without the use of site-specific and a temperature-linked mortality factors, it seems very likely that temperature and other factors played a key role in this event.

Evidence to support our model results of low-level infection from NZ-RLO1 and early infection spread in the farm populations was limited, given no valid detection of NZ-RLO1 at any of the four farms occurred prior to January 2022 (Table 5). While some NZ-RLO1 detections did occur at Waitata, these could not be validated due to cross-reactivity of PCR tests to the inactivated vaccine administered to most of the fish at that site. Given difficultly in culturing NZ-RLOs and a lack of RNA-based methods, viability assessments of bacteria were not possible using the DNA-PCR method alone. Consequently, disease diagnosis for NZ-RLO1 was supported by clinical evaluation of gross pathology, histology, DNA-PCR analysis and DNA-probe methods (data not shown).

In addition to the positive PCR detections of NZ-RLO1, *Tenacibaculum* species were also detected on the skin of moribund fish. *T. maritimum* has been isolated from moribund Chinook salmon since 2017 (Brosnahan, Munday, Ha, et al. 2019) and in 2020, *T. maritimum, T. dicentrarchi* and *T. soleae* were detected in grossly affected salmon (Table 5; Kumanan et al. 2022). *Tenacibaculum* species are a known pathogen of salmonids (Avendaño-Herrera, Toranzo, and Magariños 2006), and *T. maritimum* and *T. dicentrarchi* have been shown to be pathogenic to naïve Chinook salmon (Unpublished data: Kumanan et al. 2024). *Tenacibaculum* spp. were detected in most months and at all sites leading up to the 2022 mortality event (Table 5). Low initial mortalities at cool temperatures (i.e., October–December) suggest that tenacibaculosis did not have a large impact on fish mortality initially (Figure 2). Our model was unable to produce the highest mortality peaks observed in the data without site-specific modification of mortality to account for other stressors including coinfection (Table 2 and Figure 6). So, we hypothesise that additional stresses, including those associated with *Tenacibaculum* coinfection, likely contributed to the observed mortality peak at the worst-affected Waihinau site.

A lack of premortality event NZ-RLO1 detections, even at Waihinau site, means it is not possible to validate our model estimates of high infection prevalence, and we can only hypothesise that a low level of infection existed in the worst-affected Waihinau site prior to November 2021 (Week 10 of our simulation) (Figure 8). Consequently, the model results showing rapid infections and spread in the spring/early summer remain a working hypothesis of how bacterial infections spread during that period.

A previous challenge experiment by Brosnahan (2020) on smolt indicated limited risk to salmon from NZ-RLO1. However, a subsequent challenge experiment by Jaramillo et al. (2023) has since shown NZ-RLO1 pathogenicity in Chinook salmon via inoculation. As with genetically similar RLO strains in Tasmania (i.e., Morrison et al. 2016), when exposed to other stresses, including high temperatures, and other pathogens (i.e., *Tenacibaculum* spp. coinfection), the conditions associated with the 2022 event presented in this study show that very high mortality rates are possible.

The model was constructed using *P. salmonis* and NZ-RLO parameter ranges as an exemplar disease agent and reproduces the mortality dynamic. This provides some support for the case that NZ-RLO1 could be considered as a primary driver of mortality for the event. This is supported, in part, by expert opinion from examination of gross pathology and tests conducted from the peak of the event (data not presented here) at the worst-affected farm site, Waihinau. However, the low prevalence of NZ-RLO1 in surveillance data on moribund fish prior to the mortality event does not make for a strong case for single-infectious agent driven mortality. Indeed, at Kopaua, clinical presentation of lesions was consistent with *Tenacibaculum* spp. infection as an important driver of disease (data not shown). Given that bacterial disease parameters used in this model may fit other bacterial pathogens, we consider the modelling approach is best considered for multi-bacterial pathogen scenarios. That is, the model sufficiently covered the possibility for other pathogens, in this case inclusive of *Tenacibaculum* spp., in concert with environmental and other factors that may have had a role in this, and future, mortality events.

6 | Conclusions

The SIR disease model trained on mortality data from a summer Chinook salmon mortality event in Pelorus Sound, New Zealand, was able to reproduce observed mortality and plausible infection dynamics across three of the four salmon farms assessed in this study. Nevertheless, some uncertainty in the infection dynamics and the relative roles of the two candidate pathogens considered in this study exists due to data limitations.

The genetic similarities between NZ-RLO1 and *P. salmonis* (see Schober et al. 2023) and the model-derived parameterisations considered here show that managing future bacterial infections in a similar manner to *P. salmonis* infections provides a suitable approach. In particular, the use of vaccines appears to provide some protective benefit even though only moderate efficacy was shown in trials (Jaramillo et al. 2023) and that a relatively short immunity half-life (14 weeks) was estimated here. Based on our model results, we show evidence that vaccine use at one farm site likely prevented 10% higher mortality, and that an alternative site for the vaccination had the potential to reduce mortalities by about 20%. These results highlight the importance of future vaccine developments for bacterial pathogens in aquaculture and the potential to improve vaccine efficacy through careful site selection, if availability is limited. However, given the large *P. salmonis* issues present in Chile, and ongoing frustration with vaccine performance issues (Valenzuela-Aviles et al. 2022), further research applying the results of this model to investigate and compare other management strategies could also have long-term benefits for the NZ and other salmon farming regions.

Our modelling shows that the dynamics of bacterial pathogens in Pelorus Sound can be reproduced with a relatively simple

SIR model, provided external temperatures and site differences are considered in the formulation of mortality. This may allow future disease forecasting (if temperatures can be forecast reliably), and testing of strategies to reduce future mortalities in the area. Similarly, the effect of temperature was important in reproducing observed mortality and could be used to forecast potential future issues in a region which is subject to a clear warming trend (Broekhuizen et al. 2021). The relatively simple composition of the model also provides a useful approach for estimating epidemiological parameters for other disease events, even where limited information is available. Consequently, this approach could have wide applicability to other regions, pathogens, and host species globally.

6.1 | Future Research

The results from this study suggest that bacterial infection and associated mortality can occur very rapidly in this region. Increased disease surveillance (i.e., frequency, number of individuals and epidemiological assessment), optimised diagnostic tests, and improved and increased vaccination can mitigate future impacts of bacterial infection-related mortalities in Chinook salmon. The hindcasted infection dynamics provided by this study offer a synthetic data set that can be used to trial and quantitively assess future strategies to improve survival and welfare of cultured fish in future.

Studies from the key Atlantic salmon growing areas of Canada, Chile, Scotland and Norway show that additional factors can also contribute to disease risks in salmon aquaculture, including the following: wild species interactions (McVicar 1997; Raynard, Murray, and Gregory 2001), parasitic vectors (Almendras and Fuentealba 1997), fresh water rearing environments (e.g., Murray, Busby, and Bruno 2003; Murray 2006), seasonality and temperature (Krkošek 2010) and animal susceptibility (Fast et al. 2007). Most of these factors are either not currently considered major issues in this region, or are not easily controlled by farm managers, so have not been considered in detail for this study. However, this additional complexity could be introduced in future, if required.

Although further refinements of the approach are possible, additional complexity may lead to greater barriers to adoption and use of such tools. Consequently, it is hoped that rather than further improvements, that the framework presented here can be translated for trial use by industry. In particular, further investigations into strategies that can improve fish survival and welfare in the face of a future with increasing climate challenges should be a key focus for future study.

Author Contributions

Benjamin R. Knight: conceptualization, methodology, data curation, investigation, validation, formal analysis, visualization, writing – original draft, writing – review and editing, project administration. **Eric A. Treml:** conceptualization, methodology, writing – review and editing, supervision. **Zac Waddington:** data curation, writing – review and editing, methodology. **Ross Vennell:** methodology, software, supervision. **Kate S. Hutson:** writing – review and editing, supervision, project administration, funding acquisition.

Acknowledgements

This research was funded by the New Zealand Ministry of Business, Innovation and Employment research programmes Aquaculture Health to Maximise Productivity and Security (CAWX1707), Data Science for Aquaculture (RTVU1914) and Emerging Aquatic Diseases: a novel diagnostic pipeline and management framework (CAWX2207). We thank the staff at New Zealand King Salmon company for the collection of information and permission to use their data in this research. MetOcean Solutions are thanked for the construction of the underlying hydrological model used in the particle tracking simulations, particularly Brett Beamsley and Remy Zyngfogel. We also wish to thank Karthiga Kumanan, Andrew Robinson, Anca Hanea, Emma Hudgins and other anonymous reviewers for their helpful comments.

Conflicts of Interest

The authors declare no conflicts of interest.

Data Availability Statement

The data that support the findings of this study are available from New Zealand King Salmon Company. Restrictions apply to the availability of these data, which were used under licence for this study. Data are available from the author(s) with the permission of New Zealand King Salmon Company.

References

Abdul-Aziz, O. I., N. J. Mantua, and K. W. Myers. 2011. "Potential Climate Change Impacts on Thermal Habitats of Pacific Salmon (*Oncorhynchus* spp.) in the North Pacific Ocean and Adjacent Seas." *Canadian Journal of Fisheries and Aquatic Sciences* 68, no. 9: 1660–1680.

Almendras, F. E., and I. C. Fuentealba. 1997. "Salmonid Rickettsial Septicemia Caused by *Piscirickettsia salmonis*: A Review." *Diseases of Aquatic Organisms* 29, no. 2: 137–144.

Anderson, R. M., and R. M. May. 1979. "Population Biology of Infectious Diseases: Part I." *Nature* 280, no. 5721: 361–367.

AQNZ. 2024. "Aquaculture New Zealand Website." https://www.aquaculture.org.nz/farmed-seafood.

Avendaño-Herrera, R., A. E. Toranzo, and B. Magariños. 2006. "Tenacibaculosis Infection in Marine Fish Caused by *Tenacibaculum maritimum*: A Review." *Diseases of Aquatic Organisms* 71, no. 3: 255–266. https://doi.org/10.3354/dao071255.

Bezanson, J., A. Edelman, S. Karpinski, and V. B. Shah. 2017. "Julia: A Fresh Approach to Numerical Computing." *SIAM Review* 59, no. 1: 65–98.

Bouwmeester, M. M., M. A. Goedknegt, R. Poulin, and D. W. Thieltges. 2021. "Collateral Diseases: Aquaculture Impacts on Wildlife Infections." *Journal of Applied Ecology* 58, no. 3: 453–464.

Bravo, F., J. Sidhu, P. Bernal, et al. 2020. "Hydrodynamic Connectivity, Water Temperature, and Salinity Are Major Drivers of Piscirickettsiosis Prevalence and Transmission Among Salmonid Farms in Chile." *Aquaculture Environment Interactions* 12: 263–279.

Broekhuizen, N., D. R. Plew, M. H. Pinkerton, and M. G. Gall. 2021. "Sea Temperature Rise Over the Period 2002–2020 in Pelorus Sound, New Zealand–With Possible Implications for the Aquaculture Industry." *New Zealand Journal of Marine and Freshwater Research* 55, no. 1: 46–64.

Brosnahan, C. 2020. *Diagnostic Investigation Into Summer Mortality Events of Farmed Chinook Salmon (Oncorhynchus tshawytscha) in New Zealand: A Thesis Submitted in Partial Fulfilment of the Requirements for the Degree of Doctor of Philosophy at Massey University, Manawatū*,

274. New Zealand: Massey University. http://hdl.handle.net/10179/15278.

Brosnahan, C., H. Ha, K. Booth, A. McFadden, and J. Jones. 2017. "First Report of a Rickettsia-Like Organism From Farmed Chinook Salmon, *Oncorhynchus tshawytscha* (Walbaum), in New Zealand." *New Zealand Journal of Marine and Freshwater Research* 51, no. 3: 356–369.

Brosnahan, C. L., J. S. Munday, H. J. Ha, M. Preece, and J. B. Jones. 2019. "New Zealand Rickettsia-Like Organism (NZ-RLO) and *Tenacibaculum maritimum*: Distribution and Phylogeny in Farmed Chinook Salmon (*Oncorhynchus tshawytscha*)." *Journal of Fish Diseases* 42, no. 1: 85–95.

Bruno, D. W., P. A. Noguera, and T. T. Poppe. 2013. *A Colour Atlas of Salmonid Diseases*. Netherlands: Springer Science & Business Media.

Combe, M., M. Reverter, D. Caruso, E. Pepey, and R. E. Gozlan. 2023. "Impact of Global Warming on the Severity of Viral Diseases: A Potentially Alarming Threat to Sustainable Aquaculture Worldwide." *Microorganisms* 11, no. 4: 1049.

Cvitanich, J., O. N. Garate, and C. Smith. 1991. "The Isolation of a Rickettsia-Like Organism Causing Disease and Mortality in Chilean Salmonids and Its Confirmation by Koch's Postulate." *Journal of Fish Diseases* 14, no. 2: 121–145.

Despotovic, M., V. Nedic, D. Despotovic, and S. Cvetanovic. 2016. "Evaluation of Empirical Models for Predicting Monthly Mean Horizontal Diffuse Solar Radiation." *Renewable and Sustainable Energy Reviews* 56: 246–260.

Devesa, S., J. Barja, and A. Toranzo. 1989. "Ulcerative Skin and Fin Lesions in Reared Turbot, *Scophthalmus maximus* (L.)." *Journal of Fish Diseases* 12, no. 4: 323–333.

Fast, M., S. Johnson, T. Eddy, D. Pinto, and N. Ross. 2007. "*Lepeophtheirus salmonis* Secretory/Excretory Products and Their Effects on Atlantic Salmon Immune Gene Regulation." *Parasite Immunology* 29, no. 4: 179–189.

Handisyde, N., T. C. Telfer, and L. G. Ross. 2017. "Vulnerability of Aquaculture-Related Livelihoods to Changing Climate at the Global Scale." *Fish and Fisheries* 18: 466–488. https://doi.org/10.1111/faf.12186.

Harvell, C. D., and J. B. Lamb. 2020. "Disease Outbreaks Can Threaten Marine Biodiversity. Marine Disease Ecology." In *Marine Disease Ecology*, edited by D. C. Behringer, B. R. Silliman, and K. D. Lafferty, 1st ed., 18. Oxford: Oxford University Press.

Jamieson, P. D., J. R. Porter, and D. Wilson. 1991. "A Test of the Computer Simulation Model ARCWHEAT1 on Wheat Crops Grown in New Zealand." *Field Crops Research* 27, no. 4: 337–350.

Jaramillo, D., B. Busby, M. Bestbier, P. Bennett, and Z. Waddington. 2023. "New Zealand Rickettsia-Like Organism and *Tenacibaculum maritimum* Vaccine Efficacy Study." *Journal of Fish Diseases* 47, no. 2: 1–12.

Krkošek, M. 2010. "Host Density Thresholds and Disease Control for Fisheries and Aquaculture." *Aquaculture Environment Interactions* 1, no. 1: 21–32.

Kumanan, K., J. Carson, R. B. Hunter, et al. 2024. "Experimental Challenge of Chinook Salmon With *Tenacibaculum maritimum* and *Tenacibaculum dicentrarchi* Fulfils Koch's Postulates." *bioRxiv* 2024.03.06.583827. https://doi.org/10.1101/2024.03.06.583827.

Kumanan, K., U. von Ammon, A. Fidler, et al. 2022. "Advantages of Selective Medium for Surveillance of *Tenacibaculum* Species in Marine Fish Aquaculture." *Aquaculture* 558: 738365.

Lane, H. S., C. L. Brosnahan, and R. Poulin. 2020. "Aquatic Disease in New Zealand: Synthesis and Future Directions." *New Zealand Journal of Marine and Freshwater Research* 56, no. 1: 1–42.

Lannan, C., and J. Fryer. 1993. "*Piscirickettsia salmonis*, a Major Pathogen of Salmonid Fish in Chile." *Fisheries Research* 17, no. 1–2: 115–121.

Li, M. F., X. P. Tang, W. Wu, and H. B. Liu. 2013. "General Models for Estimating Daily Global Solar Radiation for Different Solar Radiation Zones in Mainland China." *Energy Conversion and Management* 70: 139–148.

Marcoli, R., J. E. Symonds, S. P. Walker, C. N. Battershill, and S. Bird. 2023. "Characterising the Physiological Responses of Chinook Salmon (*Oncorhynchus tshawytscha*) Subjected to Heat and Oxygen Stress." *Biology* 12, no. 10: 1342.

Marques, F. S., J. H. H. Grisi-Filho, M. Amaku, J. C. R. Silva, E. C. Almeida, and J. L. S. Júnior. 2020. "hybridModels: An R Package for the Stochastic Simulation of Disease Spreading in Dynamic Networks." *Journal of Statistical Software* 94, no. 1: 1–32. https://doi.org/10.18637/jss.v094.i06.

McVicar, A. 1997. "Disease and Parasite Implications of the Coexistence of Wild and Cultured Atlantic Salmon Populations." *ICES Journal of Marine Science* 54, no. 6: 1093–1103.

Monterey Bay Aquarium. 2020. "Seafood Watch—Chinook (King) Salmon, New Zealand." https://www.seafoodwatch.org/globalassets/sfw-data-blocks/reports/s/mba_seafoodwatch_chinook_salmon_newzealand_report.pdf.

Morrison, R., N. Young, G. Knowles, M. Cornish, and J. Carson. 2016. "Isolation of Tasmanian Rickettsia-Like Organism (RLO) From Farmed Salmonids: Identification of Multiple Serotypes and Confirmation of Pathogenicity." *Diseases of Aquatic Organisms* 122, no. 2: 85–103.

MPI. 2021. "Marine Farms Boundary Data for Current, Current Application and Declined Marine Farm Applications. Aquaculture Management Areas."

MSL. 2019. "Hindcast Hydrodynamic Modelling, MetOcean Solutions Client Report Prepared for Cawthron and MPI." Version 1.5. 70p.

Murray, A. G. 2006. "A Model of the Emergence of Infectious Pancreatic Necrosis Virus in Scottish Salmon Farms 1996–2003." *Ecological Modelling* 199, no. 1: 64–72.

Murray, A. G., C. D. Busby, and D. W. Bruno. 2003. "Infectious Pancreatic Necrosis Virus in Scottish Atlantic Salmon Farms, 1996–2001." *Emerging Infectious Diseases* 9, no. 4: 455–460.

New Zealand Government. 1991. *Resource Management Act 1991 no 69 (as at 2 April 2024)*. Wellington: New Zealand Legislation, New Zealand Government. https://www.legislation.govt.nz/act/public/1991/0069/latest/DLM230265.html.

Nowlan, J. P., S. R. Britney, J. S. Lumsden, and S. Russell. 2021. "Experimental Induction of Tenacibaculosis in Atlantic Salmon (*Salmo salar* L.) Using *Tenacibaculum maritimum*, *T. dicentrarchi*, and *T. Finnmarkense*." *Pathogens* 10, no. 11: 1439.

Olivares, J., and S. Marshall. 2010. "Determination of Minimal Concentration of *Piscirickettsia salmonis* in Water Columns to Establish a Fallowing Period in Salmon Farms." *Journal of Fish Diseases* 33, no. 3: 261–266.

Puy, A., S. L. Piano, A. Saltelli, and S. A. Levin. 2022. "Sensobol: An R Package to Compute Variance-Based Sensitivity Indices." *Journal of Statistical Software* 102, no. 5: 1–37. https://doi.org/10.18637/jss.v102.i05.

R Core Team. 2024. "R: A Language and Environment for Statistical Computing." *R Foundation for Statistical Computing*. Vienna, Austria. https://www.R-project.org/.

Rackauckas, C., and Q. Nie. 2017. "Differentialequations.Jl—A Performant and Feature-Rich Ecosystem for Solving Differential Equations in Julia." *Journal of Open Research Software* 5, no. 1: 15.

Raynard, R., A. Murray, and A. Gregory. 2001. "Infectious Salmon Anaemia Virus in Wild Fish From Scotland." *Diseases of Aquatic Organisms* 46, no. 2: 93–100.

Reid, G. K., H. J. Gurney-Smith, D. J. Marcogliese, et al. 2019. "Climate Change and Aquaculture: Considering Biological Response and Resources." *Aquaculture Environment Interactions* 11: 569–602.

Romero, J. F., I. Gardner, D. Price, T. Halasa, and K. Thakur. 2021. "DTU-DADS-Aqua: A Simulation Framework for Modelling Waterborne Spread of Highly Infectious Pathogens in Marine Aquaculture." *Transboundary and Emerging Diseases* 69, no. 4: 2029–2044.

Rozas, M., and R. Enríquez. 2014. "Piscirickettsiosis and *Piscirickettsia salmonis* in Fish: A Review." *Journal of Fish Diseases* 37, no. 3: 163–188.

Salama, N. K., and A. G. Murray. 2013. "A Comparison of Modelling Approaches to Assess the Transmission of Pathogens Between Scottish Fish Farms: The Role of Hydrodynamics and Site Biomass." *Preventive Veterinary Medicine* 108, no. 4: 285–293.

Salonius, K., C. Siderakis, A. M. MacKinnon, and S. G. Griffiths. 2005. "Use of *Arthrobacter Davidanieli* as a Live Vaccine Against *Renibacterium salmoninarum* and *Piscirickettsia salmonis* in Salmonids." *Developments in Biologicals* 121: 189–197.

Saltelli, A., M. Ratto, T. Andres, et al. 2008. *Global Sensitivity Analysis. The Primer.* Chichester, UK: John Wiley & Sons Ltd. https://doi.org/10.1002/9780470725184.

Samsing, F., I. Johnsen, T. Dempster, F. Oppedal, and E. A. Treml. 2017. "Network Analysis Reveals Strong Seasonality in the Dispersal of a Marine Parasite and Identifies Areas for Coordinated Management." *Landscape Ecology* 32: 1953–1967.

Schober, I., B. Bunk, G. Carril, et al. 2023. "Ongoing Diversification of the Global Fish Pathogen *Piscirickettsia salmonis* Through Genetic Isolation and Transposition Bursts." *ISME Journal* 17, no. 12: 2247–2258.

Stentiford, G. D., K. Sritunyalucksana, T. W. Flegel, et al. 2017. "New Paradigms to Help Solve the Global Aquaculture Disease Crisis." *PLoS Pathogens* 13, no. 2: e1006160.

Sutton, P. J., and M. Bowen. 2019. "Ocean Temperature Change Around New Zealand Over the Last 36 Years." *New Zealand Journal of Marine and Freshwater Research* 53, no. 3: 305–326.

Tsitouras, C. 2011. "Runge–Kutta Pairs of Order 5 (4) Satisfying Only the First Column Simplifying Assumption." *Computers & Mathematics with Applications* 62, no. 2: 770–775.

Valenzuela-Aviles, P., D. Torrealba, C. Figueroa, et al. 2022. "Why Vaccines Fail Against Piscirickettsiosis in Farmed Salmon and Trout and How to Avoid It: A Review." *Frontiers in Immunology* 13: 1019404.

Vennell, R., M. Scheel, S. Weppe, B. Knight, and M. Smeaton. 2021. "Fast Lagrangian Particle Tracking in Unstructured Ocean Model Grids." *Ocean Dynamics* 71: 1–15.

Wada, M., C. T. Lam, S. Rosanowski, T. Patanasatienkul, D. Price, and S. St-Hilaire. 2021. "Development of Simulation Models for Transmission of Salmonid Rickettsial Septicaemia Between Salt Water Fish Farms in Chile." *Transboundary and Emerging Diseases* 68, no. 3: 1586–1600.

Wilhelm, V., A. Miquel, L. O. Burzio, et al. 2006. "A Vaccine Against the Salmonid Pathogen *Piscirickettsia salmonis* Based on Recombinant Proteins." *Vaccine* 24, no. 23: 5083–5091.

Zhang, Y. J., F. Ye, E. V. Stanev, and S. Grashorn. 2016. "Seamless Cross-Scale Modeling With SCHISM." *Ocean Modelling* 102: 64–81.